Fuel xxx (xxxx) 124299

Contents lists available at ScienceDirect

Fuel

journal homepage: www.elsevier.com/locate/fuel

A study on biofuel produced from cracking of low density poly ethylenes using TiO_2/AlSBA-15 nanocatalysts

Kathirvel Brindhadevi [a], Bui Tat Hiep [b], Mohammed Khouj [c], Hakim AL Garalleh [d,*]

[a] Computational Engineering and Design Research Group, School of Engineering and Technology, Van Lang University, Ho Chi Minh City, Vietnam
[b] Department of Scientific Research, Cooperation and Development, School of Engineering and Technology, Van Lang University, Ho Chi Minh City, Vietnam
[c] Department of Mathematical Science, College of Engineering, University of Business and Technology, Jeddah 21361, Saudi Arabia
[d] Department of Electrical Engineering, College of Engineering, University of Business and Technology, Jeddah 21361, Saudi Arabia

ARTICLE INFO

Keywords:
Plastic fuel
TiO_2
SBA-15
TiO_2/ AlSBA-15
Interaction energy
Combination
Lennard-Jones Potential
Van der Waals force
Optimization

ABSTRACT

The burgeoning concerns over the non-biodegradable plastics wastes could be surpassed either by proper disposal technique or by an effective conversion of the plastic wastes into useful chemicals. Metal oxide; TiO_2 and porous; AlSBA-15 catalysts were synthesized and a composite characterized using XRD, BET, N_2 adsorption –desorption studies, TPD and SEM techniques. This work was focussed in the catalytic degradation of low density polyethylene over the synthesized catalysts in a fixed bed reactor. A hydrocarbon rich gasoline range of liquid fuel, coke and gas were the expected products from the experiment. The liquid products were analysed using GC MS equipped with J&W Scientific DB-Petro capillary column (100 m × 0.25 mm × 0.5 m). An optimum yield of liquid fuel was obtained with TiO_2 catalyst at 1st h of reaction and further the product yield considerably decreased. A marginal increase in % conversion of low density polyethylene into fuel was observed with increasing catalyst: polymer ratio in the presence of TiO_2 catalyst till 1:5 ratio. The liquid products contained lower range of hydrocarbons with higher content of active catalyst; while the samples collected at later stage contained heavier components. Mesoporous AlSBA-15 worked comparatively better than TiO_2 by converting 89.7% of LDPE into 54.8% combustible liquid products. The catalytic activity of the catalyst followed the order of TiO_2/AlSBA-15 (10%) < AlSBA-15 (27) < SiSBA-15 < TiO_2. A considerable increase in gasoline fraction from 45.6% to 85.4%, yield of liquid fuel (89.1%) and conversion (98.4%) was observed during cracking in the presence of TiO_2/AlSBA-15 catalyst. Plastic liquid fuel produced over the composite catalyst revealed the calorific value of 47.8 MJ/Kg which was higher than the commercial petroleum fuel. Finally, we obtain this biofuel application as mathematical model to evaluate and plot the interaction energy arising from the conjugation of TiO2 – AlSBA-15 nano-catalyst in two possible configuration, linear (conical) and spherical molecules, along the range of the α distance $(z - axis)$.

1. Introduction

Plastics have become an integral part of our life and imagining a modern society without them should be far from reach. The reason for the dominance of this non-biodegradable polymers constituted mainly by Carbon and Hydrogen in industrial and domestic sectors are their features such as light-weight, durable, energy efficient, flexible for desired design [1,2]. However, their non-decomposing nature imposes a bigger threat to Municipal waste management. According to the world statistics, about 381 million tonnes of plastic waste is generated annually; which could double by 2034 [3]. Single-use plastics constitute around 50% and only 9% has ever been recycled. The most common plastic communities are polyethylene terephthalate (PET), High density polyethylene (HDPE), Poly vinyl chloride (PVC), Low-density polyethylene (LDPE), Polypropylene (PP), Polystyrene (PS) [4,5]. The poor mechanical recycling index of LDPE, which is commonly used in packaging films, causes a slew of environmental issues as well as issues with disposal [6].

Incineration and landfilling are no longer viable solutions because the former emits poisonous gases that pollute the air, while the latter necessitates a large amount of landfill space when compared to biodegradable trash [7,8]. Conversion of plastics to the clean burning

* Corresponding author.
E-mail addresses: brindhadevi.k@vlu.edu.vn (K. Brindhadevi), hiep.bt@vlu.edu.vn (B. Tat Hiep), m.khouj@ubt.edu.sa (M. Khouj), ha764@uowmail.edu.au (H. AL Garalleh).

https://doi.org/10.1016/j.fuel.2022.124299
Received 19 November 2021; Received in revised form 4 April 2022; Accepted 19 April 2022
0016-2361/

hydrogen, an alternative motor fuel; diesel, crude oil and sulphur are the most happening research in the recent decade [9,10]. For a successful commercial future, recycling/conversion of plastics into utility materials perhaps are the better idea. The idea of disposing of plastics by producing alternative liquid fuels is extremely welcome, given the combustion of fossil fuels has resulted in alarming air pollution and rapid resource depletion [11–13]. An alternative liquid fuel with physicochemical qualities similar to petro-fuels should be long-lasting, environmentally safe, and inexpensive [14,15]. Thermal degradation or thermo catalytic degradation would provide the alternate potential way for disposal these hazardous materials with recovery of liquid alternative fuels [16]. Petroleum products manufactured from plastics have a high calorific value (46,500 KJ/kg), which is a potential factor for using them as a sustainable resource. Regardless of whether the cracking occurs with or without a catalyst, the process produces liquid hydrocarbons with boiling points ranging from 40 to 350 °C, gas, coke, and wax. In a lab scale semi-batch reactor, Das and Tiwari [12] demonstrated slow pyrolysis of low and high-density polyethylene and polypropylene at a very slow dynamic condition (1 °C min^{-1}). As the pyrolysis reactor temperature approached its maximum value (400 °C), the yield of both the light and medium fractions dropped.

Among the other primary components of gases, propylene was found to have a greater dominance. Several works have been published reporting the excess gas emitted from pyrolysis of plastics [17–20]. Although gaseous products can help meet the energy demands of an endothermic polymer cracking process, too much gas production is undesirable. Because of the high expense of delivery, the gaseous items are seen as low-value [21]. As a result, an increase in the liquid product yield should be the goal of any commercially successful recycling process. Thermal degradation is a less desirable option since it necessitates quite high temperature, requires additional processing to improve product quality and yields high % of gas [22]. Nitrous oxides, sulphur dioxides, particulate matter, and other hazardous pollutants can be released when plastic is burned [23]. Catalytic degradation of plastic waste, on the other hand, has several advantages, including lower working temperatures, low greenhouse gas emissions, reduced activation energies, faster rates, and low energy requirement compared to gasification and pyrolysis, and the formation of hydrocarbons similar to those found in motor engine fuel, obviating the need for further processing [24]. However, the process draws concern over uncontrolled C–C bond breakage at high temperatures and lengthy periods of time. Zeolites are crystalline alumina silicates having a restricted pore range, good thermal stability, and high specificity. By incorporating aluminium into the silica lattice, the acidic character of zeolite can be considerably improved. Some of the factors to consider are catalyst residence time, acidity, porosity, and pore size.

The next version of these silica aluminates are the mesoporous materials with pore diameter in the range of 2 nm – 50 nm. The application of mesoporous materials in cracking feedstocks into specific products has enlarged in the recent years. The flexible porous nature, pore size channelling and moderate cracking ability are the most appreciable qualities of these materials. MM 41S family of materials are widely utilized for industrial applications including petroleum processing, fine chemical synthesis and adsorption studies. MCM-41, MCM-48, SBA-15 etc. Yet another, class of catalysts that are establishing their catalytic activity due to their outstanding properties such as a) easy synthesis b) simple structure c) abundant availability are transition metal oxides ex. ZrO_2, NiO_2, TiO_2 [20,25,26] etc. TiO_2 is a naturally occurring metal oxide that can be used to catalyse waste plastic pyrolysis. Titanium dioxide is made up of natural minerals such ilmenite, rutile, and anatase, all of which include titanium. Titanium dioxide can be used as a pigment to provide whiteness and opacity to paint coatings, plastics, and paper due to its high refractive index. It can be used to make thin films and to block UV light. Titanium dioxide is commonly used to stabilise heterogeneous catalysts. Degradation of plastics are mostly carried out over solid acid catalysts; zeolites (HY, HZSM-5, HMordenite) and mesoporous MCM-41 [27–29], composites- MCM41/ZSM-5 [30,31], clay pillared materials, silica aluminates, oxides (CaO, ZnO, ZrO_2) and activated Carbon [32].

Researchers at the University of California, Santa Barbara, developed SBA-15, a highly stable mesoporous silica sieve. Its high hydrothermal and mechanical stability comes from a framework of uniform hexagonal pores with a narrow pore-size distribution and a tunable pore diameter of 5 nm to 15 nm, as well as its relatively thick walls, which range between 3.1 nm and 6.4 nm. The high internal surface area of SBA mesoporous silica 15 lends itself to a variety of applications, including adsorption, catalysis and optical study. Sterically challenging high density poly ethylene was cracked using AlSBA-15 by Socci et al. [33] racking of polypropylene over Fe-SBA-15 was proposed by Zhao et al. [34] to yield light hydrocarbon oils. Munir and Usman [35] cracked mixture of plastics using composite USY/SBA-16 catalyst and the results pronounced the improved activity of composite over parent USY catalyst. In this research, optimizing the reaction conditions were done using TiO_2 catalyst and the catalytic efficiency of SBA-15 and Al-incorporated AlSBA-15 was further examined. Further, TiO_2 /AlSBA-15 were investigated to understand the catalytic efficiency.

2. Materials and methods

TiO_2 was synthesized using Analytical graded Titanium-isopropoxide procured from Sigma-Aldrich with > 97 % purity. Tea powder was prepared in the laboratory from Tata 3 roses tea packet purchased from local market.

2.1. Synthesis of TiO_2 NPs

Tea decoction was prepared by boiling the 50 g of tea powder in 150 mL of distilled water and separated using whatman filter paper grade No 1- size 110 mM. The distillate was collected and stored in a sealed vial in refrigeration condition. 100 mL Titanium isopropoxide solution (5 mM) was added to 100 mL tea decoction in a 1:1 (v/v) ratio, followed by 6 h of continuous stirring at room temperature. The hydrolysis of Titanium isopropoxide, which was the major pathway for the creation of TiO_2 NPs, was the mechanism behind their formation. The tea decoction in the solution mixture served as a stabilising agent, preventing agglomeration and allowing the TiO_2 NPs to reach the required shape and size. To separate the nanoparticles, the liquid was centrifuged at 7000 rpm for 7 min after stirring. Wet powdered TiO_2 NPs were obtained and dried overnight at 100 °C before being calcined for 3 h at 600 °C in a muffle furnace.

2.2. Synthesis of porous SiSBA-15

The synthesis procedure of SiSBA-15 is already reported in our earlier research article [36]. The composition of the obtained gel was: 0.5 TEOS: 0.0085 P123: 2.84 HCl: 98.5 H2O. Pluronic P123 (EO20PO70O20), a non-ionic tri-block copolymer, was dissolved in hydrochloric solution in a 250 mL polypropylene beaker at 40 °C. The surface directing agent, TEOS was slowly introduced into the medium maintained at 40 °C under continuous stirring for 2 h. The hydrothermal synthesis of catalyst was performed at 100 °C for 24 h in a hot air oven in a sealed polypropylene bottle. Filtration of the product mixture using Büchner filter followed by washing with distilled water and overnight drying resulted in solid mass.

2.3. Wet impregnation of aluminium ions onto the SBA-15

Wet impregnation was used to load Ca^{2+} ions into SBA-15, a mesoporous material. To 2 g of the synthesised SBA-15 catalyst, 75 mL of 0.1 M aluminium sulphate solution was added. The mixture was

swirled for 2 h at 60˚celsius using a hot pad magnetic stirrer. The resulting solution was filtered, and the solid material was thoroughly rinsed with distilled water before being dried at room temperature. For cracking reactions, several loadings of Al^{3+} (3 to 1 wt%) on SBA-15 were synthesised and employed.

2.4. Synthesis of nano composite TiO_2/AlSBA-15

A variety of TiO_2/SBA-15 nanocomposites were also made using a modified implantation approach, with the detailed methods presented below. In 40 mL of n-hexane, 2.8 mL of tetrabutyl titanate was dissolved. 2.0 g of AlSBA-15 powders were mixed into the above combined solution after 10 min of stirring to produce a suspension. At 60 ˚C, the mixture was continually mixed until a fine powder formed, and the powders were promptly placed in an oven and heated to 150 ˚C for 3 h. The powder was then dispersed in n-hexane, filtered, and dried at 100 ˚C. The product was utilised as the carriers to repeat the previous stages in order to increase the content of TiO_2 in TiO_2/SBA-15 nanocomposites. Finally, the four products were calcined for 4 h at 500 ˚C to produce four TiO_2/AlSBA-15 nanocomposites, which were labelled TS-1 (5%), TS-2 (10%) and TS-3 (15%), respectively.

2.5. Characterization techniques

XRD measurements were performed on the Bruker D8 advance diffractometer operating in the reflection mode with Cu-Kα radiation (35 kV, 30 mA) and diffracted beam monochromator, using a step scan mode with the step of 0.075˚ (2θ) and 4 s per step. Composite Nanomaterials were recorded at both low angle and high angle. Transmission electron microscopy was used to study the morphology and mesoporous structure of the samples (TEM, JME- 1200EX). An energy dispersive spectrometer (EDS: TEAM Apollo XL) linked to the scanning electron microscope was used to investigate the elemental analyses (SEM). Brunauer-Emmett-Teller (BET) specific surface area, pore diameter, and pore volume were determined using N_2 physisorption at 196 ˚C on a micrometrics ASAP 2020 surface area and porosity analyzer after the samples were degassed under vacuum at 250 ˚C for 4 h. The acidity studies were performed using NH_3-temperature programmed desorption in Chemisorb 2720 (Micrometrics, USA) instrument equipped with a TCD detector. To evaluate pyrolysis, LDPE sample was decomposed more between 400 and 450 ˚C (under an inert atmosphere of pure nitrogen with a flow rate of 15 ˚C min^{-1}) in TGA (209 F3, NETZSCH Co.,Bavaria, Germany). As a result, the instrument's temperature was set to 450 ˚C. This is excellent for studying the thermal stability and behaviour of LDPE in an inert environment.

2.6. Degradation of LDPEW into biofuel

Catalytic pyrolysis was used on the polyethylene film samples. Fig. 1 depicts the installation process flowchart. The reactor was a horizontal batch reactor (Naberthem). To provide an inert atmosphere, a steady nitrogen stream of 100 mL/min was supplied into each experiment. In each experiment, an aluminium container containing around 20 g of pellet and the appropriate amount of catalyst was fed into the reactor, and this feed remained as a fixed bed throughout the experiment. Temperature of 450 °C, a heating ramp of 20 °C min^{-1}, and a residence time of 120 min were used in the experiments. These experimental conditions were chosen based on the findings of a previous study. This mixture was homogenised for 10 min at 300 rpm prior to the insertion of the pellet-catalyst sample. The majority of the studies employed a 10% wt catalyst. In order to check the effectiveness of the parameter, different catalyst ratios of 5 to 20% wt of catalyst were utilised for some catalysts. The polyethylene trash began to decompose after the pyrolysis process began. As the experiment progressed, a stream of gases emerged and passed through a condenser, an ultrathermostat that allowed these streams to be cooled to 4 ˚C. With the help of the nitrogen stream, the volatile products were transported from the reactor to the condenser. The gaseous fraction, which is the non-condensable phase, and the liquid fraction, which is the condensable phase, was separated after the condensation process was completed. At atmospheric conditions, the yield of products was calculated using the formula:

$$\%\text{ofPLFobtained}\frac{Weightofoil(g)}{Weightofplastictaken(g)} \quad (1)$$

GC (Agilent-7890) fitted with FID detector was used to identify presence of gasoline, kerosene and diesel fractions. The quantification of individual fragments was determined by using Mass spectrum make model Jeol Accu TOF GCV with mass range 10–1500 amu and mass resolution 5000. ASTM standards proposed for analysing the alternative liquid fuels were followed and the analysis was done Tamil Nadu testing house in Chennai, India.

3. Results and discussion

3.1. XRD analysis of the synthesized catalysts

Fig. 2 (a,b) shows the characteristic peaks of AlSBA-15, TiO_2 and TiO_2/AlSBA-15 materials obtained from XRD analysis. Fig. 2a shows XRD patterns with significant diffraction peaks at 27°, 36 °, and 55°, suggesting TiO_2 in the rutile phase. The conventional spectrum agrees with all of the peaks (JCPDS no.: 88–1175 and 84–1286). These findings indicated that the nano-TiO_2 powder is made up of uneven polycrystalline particles. The influence of amorphous materials on the widening of the XRD patterns of nanosized TiO_2 is insignificant. The narrow peaks can be seen that confirms the crystallinity of the catalysts. The powder XRD pattern of SBA-15 (Fig. 2b) shows three peaks, which is a basic property of every hexagonally organised material. The peaks were indexed at [1 0 0], [1 1 0], and [2 0 0] reflections, which corresponded to peaks between 2.0 and 2.5˚. For the synthesised mesoporous SBA-15 material, Shi et al. [37] obtained the same diffraction peaks. The substantial peak around 2.5, on the other hand, correlates to SBA-15′s highly organised porous structure. Aluminium-impregnated SBA-15, on the other hand, had slightly deformed peaks that were displaced to higher angles. The loading of Al^{3+} ions on SBA-15 was increased from 2 to 10% wt%, resulting in low intensity peaks and peaks displaced to a higher angle order. The d spacing values were estimated using Bragg's equation ($n = 2d\sin\theta$), and the unit cell constants were computed using the equation $a0 = 2d100/3$ for all AlSBA-15 catalysts (Table 1). The mesoporous nature of the produced catalysts is seen in these peaks. According to Wan et al. [38], when the aluminium concentration increased, the peak intensity reduced and shifted towards higher 2θ values. With a lower Si/Al ratio, the [1 0 0] diffraction peaks expanded slightly and became less intense, which could be owing to a shift in the T-O-T bond angle, causing long-range order distortion in the hexagonal mesoporous structure. The strongest peak corresponding to the (1 0 0) plane was likewise identified in the patterns when TiO_2 nanoparticles were incoporated into SBA-15, and the peak intensities of TiO_2/AlSBA-15 nanocomposites steadily declined with increasing TiO_2 nanoparticle loading (Fig. 2c). Two further weak peaks, in particular, could only be found in the pattern of TS-1. According to the foregoing findings, TiO_2 nanoparticles entered the AlSBA-15 mesopores and partially blocked them.

3.2. TEM images of the synthesized catalysts

TEM studies investigated the morphology and crystalline nature of TiO_2, SBA-15 and composite TiO_2/SBA-15 catalysts. Spherical shapes of TiO_2 with a grain size of 0.3–0.7 μm are well observed in Fig. 3a in TEM bright field image which is characteristic feature of rutile phase. Well-ordered particles of 10 nm size can be noted which is consistent with

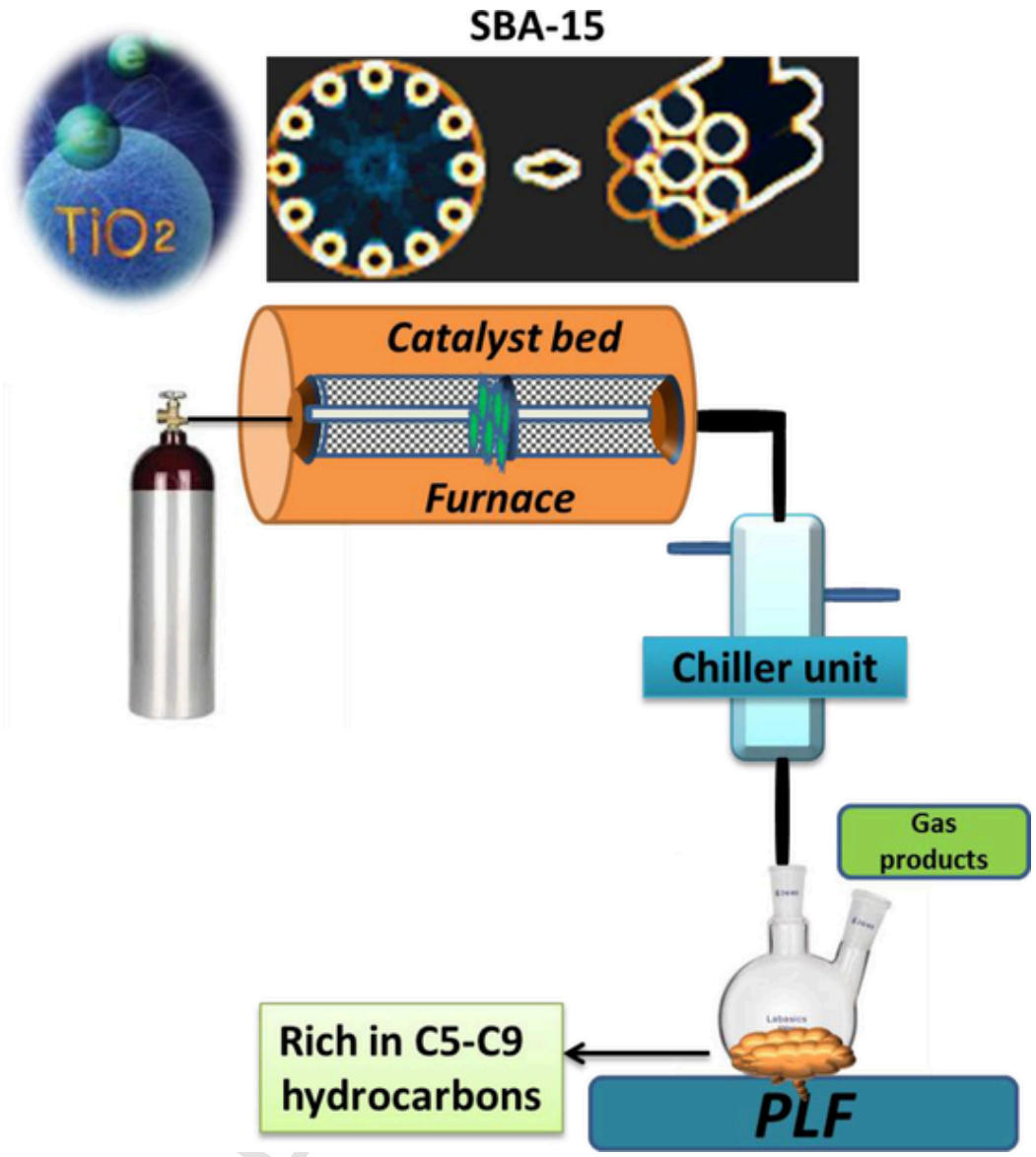

Fig. 1. Experimental set up of the LDEW cracking.

the XRD results. Fig. 3b displays the uniform arrangement of hexagonal mesochannels of SBA-15 which is uninterrupted with the incorporation of aluminium ions into alumina silicate lattice. The successful insertion of 'Al' into the lattice were demonstrated by Kolli et al. [39]. The study affirms the stability of the material for industrial purpose. The composites prepared using TiO_2 and SBA-15 revealed deep insertion of TiO_2 in the mesoporous lattice (Fig. 3c). Perhaps, a slight deformation of mesoporous lattice is an evidence for the core–shell formation. However, Guo et al. [40] reported the un altered XRD peaks position in TiO_2@SBA-15 composites.

3.3. N_2 Adsorption desorption and temperature desorption studies

The surface areas of the mesoporous AlSBA-15 improved as the materials' aluminium concentration decreased (Table.1). This pattern was discovered to be compatible with previously published literature. AlSBA-15 (1 0 0) has the largest surface area of 1067 m^2/g among the AlSBA-15 with varying Si/Al ratios. With more aluminium in the lattice, the structure distorts, resulting in a smaller surface area. With the implanting of TiO_2 nanoparticles into the mesopores, the BET specific surface area reduced dramatically from 948 $m^2/$ g to 756 m^2/g for TS-1. To analyse the mesoporous-structure of SBA-15, TiO_2/SBA-15 nanocomposites, and TiO_2, the nitrogen adsorption and desorption isotherms in Fig. 4 (a-c) respectively were used. According to the IUPAC convention, the isotherms of SBA-15 could be classed as type IV and had the characteristic H1 hysteresis loop, showing that SBA-15 had a homogeneous mesoporous structure. Similarly, type IV isotherms were observed in the TS (1, 2 and 3) nanocomposite, implying that the mesostructure of SBA-15 was preserved following the loading of TiO_2 nanoparticles, which was compatible with the TEM observation.

The hysteresis loops were more probable of the H_2 type, notably for all composites, implying that the larger TiO_2 nanoparticles occupied the mesopores via multistep impregnation. Furthermore, the hysteresis loops of nanocomposites switched to lower relative pressures, meaning that the average pore size shrank as TiO_2 nanoparticles increased, which was consistent with the observation from Fig. 4b. Marques et al. [41] reported the surface area of TiO_2 to be 228 m^2/g which was comparable to the synthesized material (256 m^2/g).In addition, the TiO_2 curve showed IV-type adsorption isotherms, which is a mesoporous material feature. Jaroszewska et al. [42] studied hydroisomerization of long chain n-alkanes over Pt/AlSBA15 and the synthesized catalyst

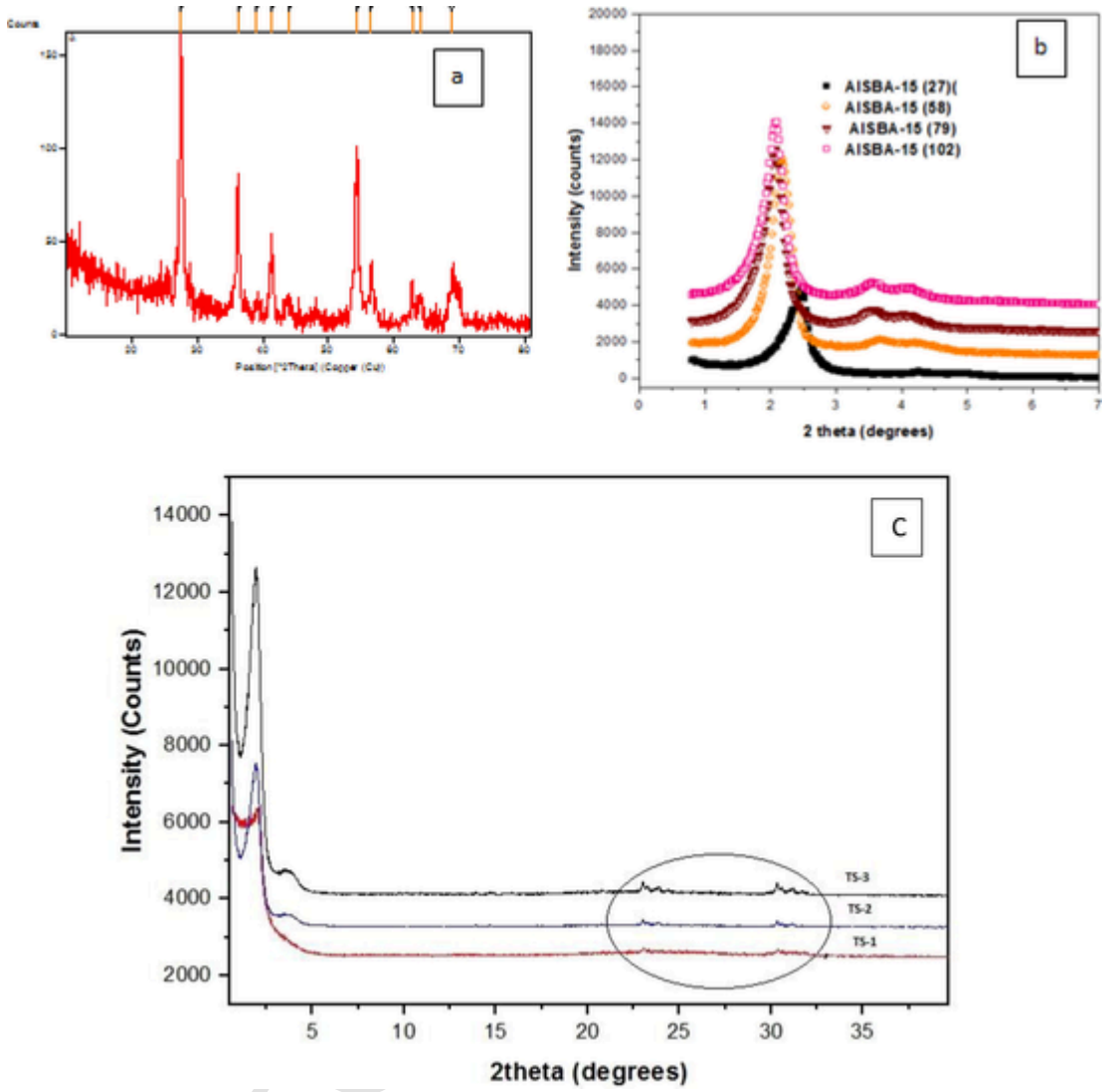

Fig. 2. XRD patterns of the synthesized catalysts a) TiO_2 b) AlSBA-15 of different Si/Al ratio and c) Presence of mesoporosity in Nano composite TS-2.

Table 1
Characterisation results of catalyst.

Catalyst	XRD		Acidity (μmol/g)	BET Surface area
	d (nm)	Unit cell parameter (a_0) (nm)		
AlSBA-15 (25)	3.58	4.13	38.0	497
AlSBA-15 (50)	4.09	4.72	37.5	625
AlSBA-15 (75)	4.20	4.84	37.0	810
AlSBA-15 (1 0 0)	4.20	4.84	36.8	967
TS 1	4.50	5.19	20.1	756
TS 2	4.47	5.16	31.2	789
TS 3	4.46	5.15	33.1	899
TiO_2	7.52	10		68

showed similar hysteresis loop corresponding to the Mesoporous nature of the materials.

3.4. EDX of the synthesized catalysts

EDX was used to characterise the components of TiO_2/SBA-15 nanocomposites in comparison to SBA-15 and TiO_2 (Fig. 5). The presence of Si, Al and C should be attributed to AlSBA-15. The element Ti was also present in all TiO_2/SBA-15 nanocomposites. Similar EDX graphs are published elsewhere [43,44].

3.5. Optimization studies for cracking LDPEW into biofuel using TiO_2 catalyst

3.5.1. Thermogravimetric analysis of LDPE

Fig. 6 shows the thermogravimetry analysis (TGA) curve. The TGA of the LDPE was determined in a nitrogen atmosphere. It shows that beyond 400 °C, LDPE begins to degrade and completely transforms into a gaseous phase, with no solid mass left over 500 °C [45]. Zheng et al. [46] studied LDPE degradation by TGA analysis and observed degradation plastics between 400 °C and 500 °C. The degradation studies declare that the conversion of plastics into liquid fuel can be performed in the mentioned temperature range. The cracking of LDPEW above 500 °C would lead to deformation of the chemical compo-

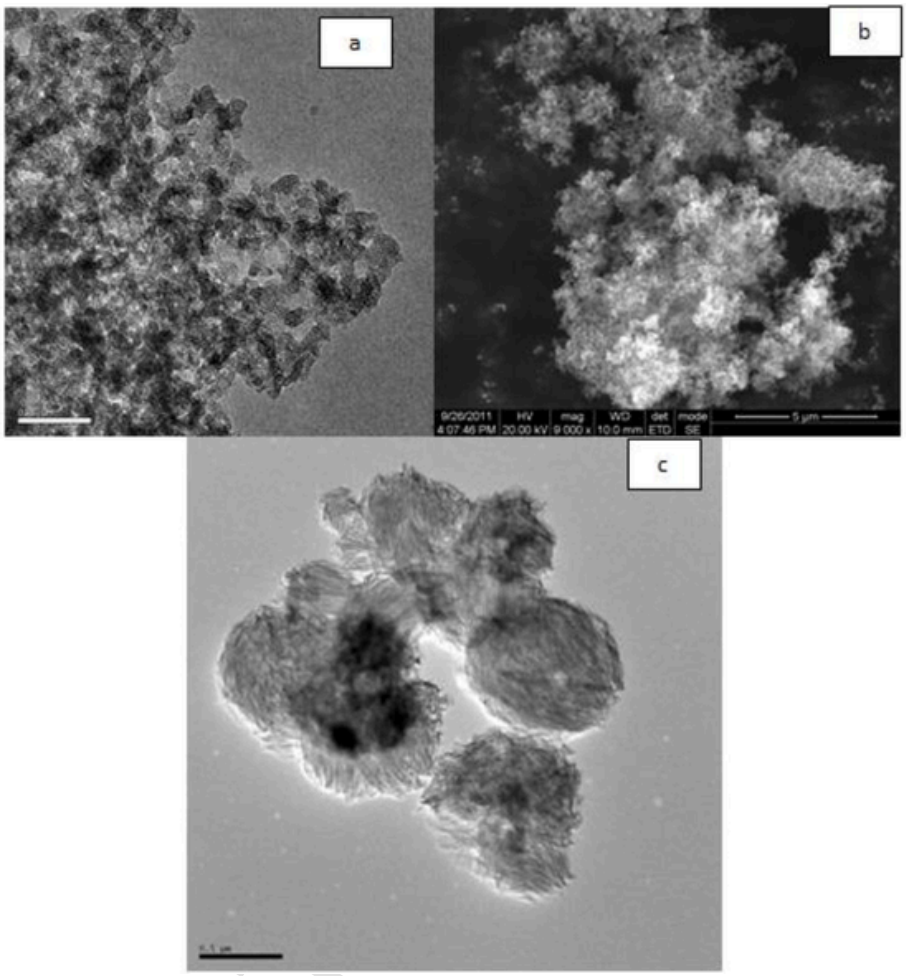

Fig. 3. TEM images of synthesized catalysts a) TiO_2 b) AlSBA-15 (25) and c) TiO_2/AlSBA-15 (10 %).

sition of the material. Therefore, the cracking reactions should not exceed 500 °C for obtaining better fuel.

3.5.2. *Effect of time on the yield of biofuel*

Fig. 7 provide the effect of time on conversion of LDPEW into PLF at different time intervals. In order to eliminate the coking of catalyst, a continuous supply of inert N_2 gas was constantly passed through the reactor. The decomposition of LDPEW started within the first 5th min of the reaction which was evident from the liquid gaseous products entering the condenser. The products collected for the first 5th min were discarded and collection was done in the time interval of 30 min from 0.5 h to 2.5 h. The conversion was found to increase with increase in time from 0.5 h to 1 h in the presence of TiO_2. However, the conversion witnessed a drop with further increase in reaction duration. The physical deposition of undesired carbonaceous species from the liquid feed over the active site of catalyst causes activity loss due to the clogging of active pores. The deactivation of the catalyst during the course of the cracking process was observed to be the major drawback [47, 48].

3.6. *Cracking efficiency study: Thermal cracking vs TiO_2 cracking of LDPEW*

3.6.1. *Thermal cracking vs catalytic cracking of LDPEW*

The Table 2 compares the conversion of plastics into PLF with TiO_2 and without catalyst at the optimized reaction condition. Conversion of plastics was found to increase steeply when the cracking was carried out in presence of the composite catalyst. The conversion was found to increase irrespective of the catalytic condition showing the influence of temperature on cracking plastics. Besides, the increase in conversion, the yield of liquid fuel dropped with increasing pyrolysis temperature. Thermal and catalytic cracking exhibited drop in liquid fuel yield. Further, there is increase in yield of gaseous products during the reaction. Wang et al. [49] compared cracking of vegetable oil soapstock in the presence and absence of catalyst, and, maximum yield of liquid fuels was obtained from catalytic cracking of feed.

3.6.2. *Effect of catalyst content vs yield of PLF*

As expected catalyst showed great impact on the conversion of oil into desirable products (Table 3). Higher as well as lower concentration of catalyst found to be unfavourable due to either excessive cracking leading to high % of gas or poor cracking efficiency resulting in unvolatalized plastic residues. The plastic residues would block the active sites of the TiO_2 catalyst. The catalyst:polymer ratio of 1:5 provided better conversion (75.3%) and PLF (40.6%). Nwankwor et al.[28] on cracking of waste plastics using TiO_2 catalyst also proposed that conversion increased with increase in catalytic concentration and observed the decrease in conversion with further increase in catalytic conversion.

3.6.3. *Cracking activity of the synthesized catalysts*

Fig. 8 shows the conversion, yield of plastic liquid fuel and selectivity of gasoline fraction. The composites were far better than the parent TiO_2 and AlSBA-15 materials. Similar kind of better activity of composite catalysts over the precursor materials for cracking vegetable oils such as triglycerides, soyabean oil were proposed by Vu et al.[50], Shirasaki et al. [51] and Ganesan et al. [52]. Composite of

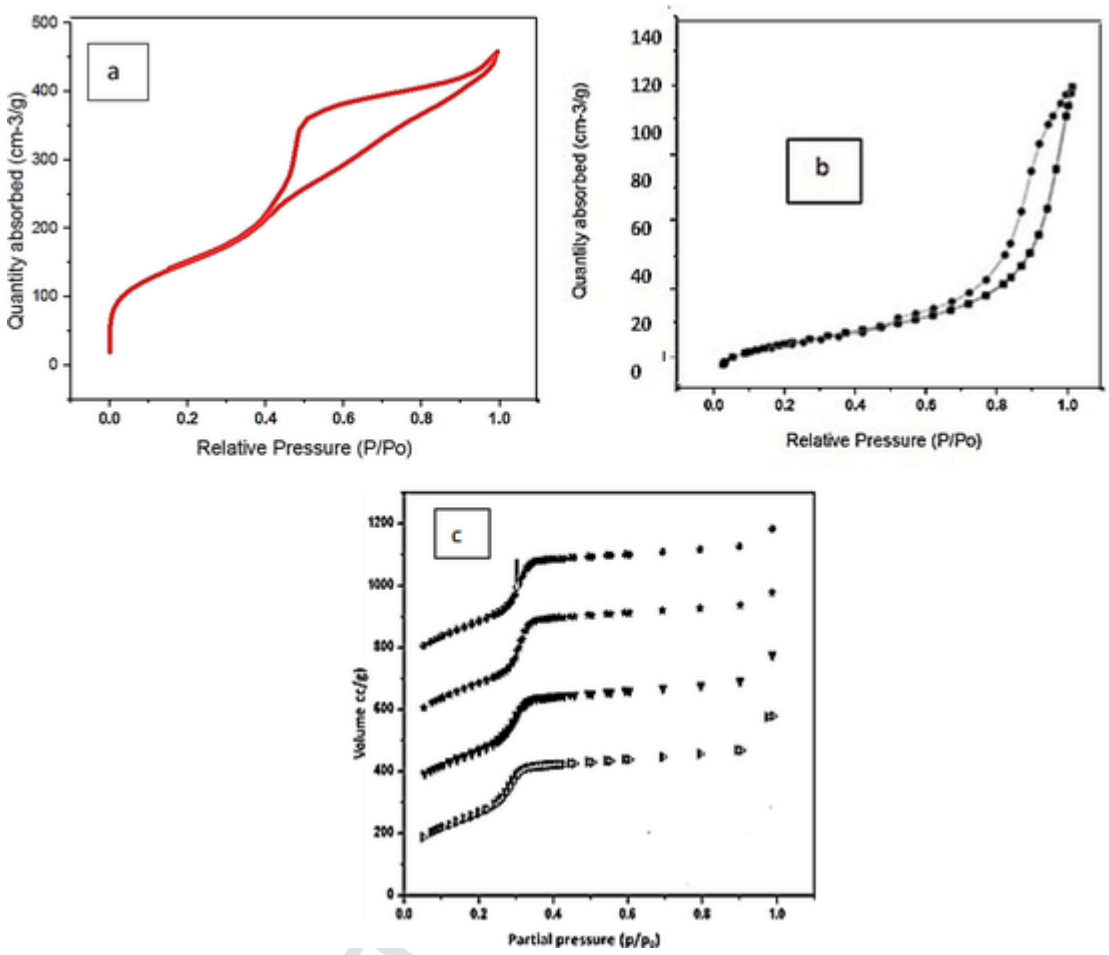

Fig. 4. Adsorption and desorption of a) AlSBA15 (25), b) TiO_2 and c) Nano composite TS 2.

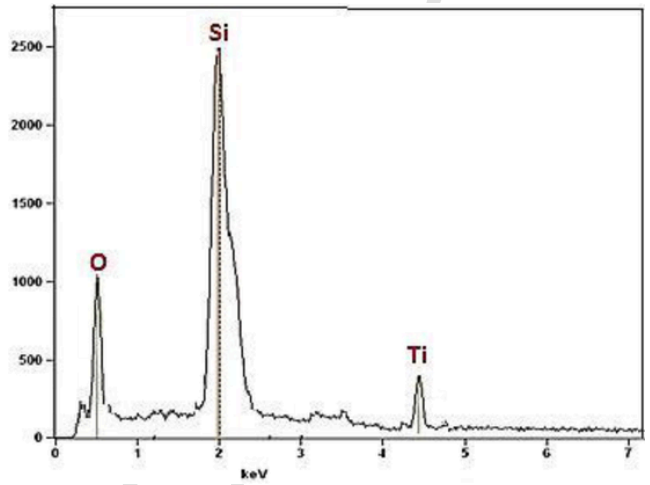

Fig. 5. EDX of TS-2.

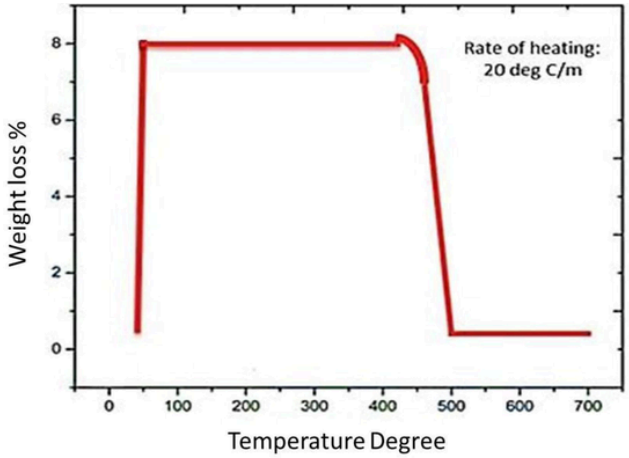

Fig. 6. Thermo gravimetric analysis of LDPEW used for the study.

TiO_2 and mesoprous material has been reported for the production of biodiesel from vegetable oils [53] and biohydrogen [54]. The following observations were made from the obtained results:

a) A better conversion of LDPEW into liquid products was obtained using the mesoporous material AlSBA-15 compared to TiO_2. The higher surface area (400–600 m^2/g) and better acidity range of AlSBA-15 (in the range from 30 to 40 μL/g) should be the reason for the observation. Further, the porous nature of SBA materials is supportive for the cracking reactions. The importance of high surface area of porous materials was proposed by Trisunaryanti et al. [55] in converting *Calophyllum inophyllum* oil to biofuel.

b) The increase in Aluminium incorporation in SBA-15 catalyst seen a notable increase in conversion of plastic liquids into liquid fuel. However, there was a decrease in conversion with further increase in Aluminium incorporation AlSBA-15 (25). Hu et al. [56] studied the role of acidity in converting oleic acids into fuel over MgO, CaO and TiO_2 catalysts. Incorporation of acidity into catalytic materials was observed to increase in efficiency of the catalysts.

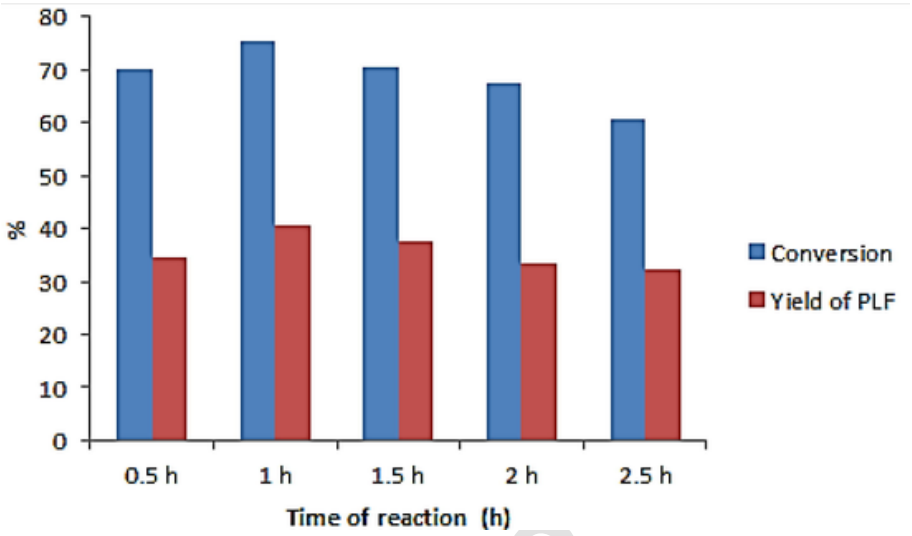

Fig. 7. Effect of time on product yield.

Table 2
Conversion and yield of products at varied temperatures.

	Thermal cracking			Cracking using TiO_2		
	400 °C	450 °C	500 °C	400 °C	450 °C	500 °C
Conversion (%)	35.5	55.6	45.	48.4	73.5	60.7
Yield of PLF (%)	25.7	30.8	26.7	31.3	37.8	34.3
Yield of char, gas and water (%)	9.8	24.8	18.3	17.1	26.7	26.4

Table 3
Polymer:catalyst ratio vs Conversion.

Polymer:catalyst ratio	Conversion (%)	PLF yield (%)
1:1	70.3	36.7
2:1	73.4	37.7
3:1	74.6	38.3
4:1	74.6	39.1
5:1	75.3	40.6
6:1	73.5	37.8

*Reaction @450 °C.

c) Composite materials worked efficiently in cracking the LDPEW into higher quantity of liquid products invariant of the % coating of TiO_2. The highest conversion was given by 10 % coating (TS-2) (98.4% conversion, 89.1% PLF and 85.4% selectivity) among the 5, 10, and 20% TiO_2/AlSBA-15 coatings. The conversion increased when the % coating of mesophase was increased to 10%, but as the % coating of mesophase was increased to 20%, the conversion declined. Because of the increased coating of mesoporous material on TiO_2, the active sites of zeolite are blocked, resulting in decreased conversion. However, the cracking activity of TiO_2 and AlSBA-15 were also convincing compared to the composite material. Cao et al. [57] synthesized MgO and ZnO/SBA-15 composites and employed in converting waste cooking oils into liquid hydrocarbon fuels. About 37.3 % of bio liquid fuel was obtained using ZnO/SBA-15 composites.

d) The gasoline fraction is found to be highest in the liquid fuel obtained using composite material; TS-2. Composite materials yielded least % of higher range of hydrocarbons as reported by Cao et al. [57].

3.6.4. Comparison of PLF through pyrolysis and catalytic cracking using GC MS

The standard used for identifying the hydrocarbons present in the PLF was the commercially available gasoline, kerosene and diesel. Table 4 gives the RT of major constituent of commercial fuel fractions

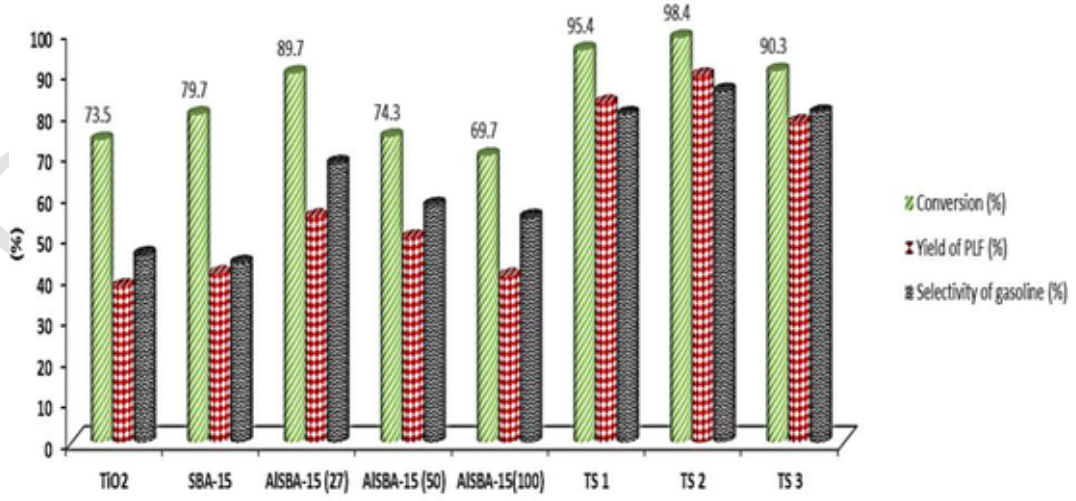

Fig. 8. Cracking efficiency of the synthesized catalysts TS-1- TiO_2/SBA-15(5%), TS-2- TiO_2/SBA-15(10%) and TS-3- TiO_2/SBA-15(20%).

Table 4
GC analysis of fuel standards.

Sample	No	RT [min]	Area [mV*s]	Area%	Height [mV]
Diesel	1	7.3333	701.3546	25.28	4.6618
	2	8.1667	2072.444	74.72	9.9138
	3	9.2377	753.6578	27.16	5.0094
Gasoline	1	0.7333	636.0912	8.83	72.6751
	2	0.9	586.3674	8.14	73.2074
	3	1.0667	1947.349	27.03	107.7883
	4	1.7667	3064.142	42.54	80.1577
	5	2.7833	728.4805	10.11	18.5872
	6	3.4833	241.2561	3.35	12.1077
Kerosene	1	5.0333	701.3546	25.28	69.36
	2	8.1667	2072.444	74.72	12.57
	3	9.2377	753.6578	27.16	11.62

which was used for comparison. Fig. 9 shows the pyrolysis of LDPEW produced liquid fuels with wide range of hydrocarbons whereas in catalytic cracking, the hydrocarbon range was desirable range mainly constituting gasoline range (>C-18). PLF peak at 0.9 may correspond to the recorded value of commercial gasoline which corresponds to lower hydrocarbons (C4). Whereas such peaks is not attained in analysis of pyrolyzed liquids as well as commercial diesel. The gasoline standard peak at RT 3.4833 can be observed in the PLF produced using composite material. The standard corresponds to branch lower hydrocarbons (Alkyl substituted C5 chain) the lack of intensive and specific cracking is obvious from the peaks of C16 chain hydrocarbons observed in thermally cracked liquid. Presence of aromatics substituted aromatics and poly aromatic compounds in catalytically cracked liquid can be identified from the peaks around 6.50–6.8 RT. Isomerization and cyclization reaction occurring in the porous channels should be the reason the formation of cyclic products. Yousef et al. [58] investigated the pyrolyzed fuel obtained from low density plastics using GC MS and observed the longer chain hydrocarbons in diesel range. Fe/HZSM-5 catalyst was employed by Dwivedi et al. [59] to perform two-step cracking to produce 66.39 % of C6-C20 hydrocarbons.

3.7. Physico-chemical analysis of catalytically cracked PLF vs pyrolyzed PLF

The four important characteristics of fuel, including flash point, density, heating value and viscosity were studied for pyrolyzed plastic oil and catalytically cracked PLF (TiO_2 and AlSBA-15) and given in Table 5. The calorific value of a fuel is one of the most essential characteristics used to assess its efficiency. The calorific value is the amount of energy released when a unit mass of fuel is completely burnt in adequate air. TiO_2 - PLF calorific value was found to be 45.7 MJ/Kg. The value was better compared to the pyrolyzed plastic fuel and comparable with the commercial petrol. AlSBA-15- PLF inhibited the best heating value of 67.8 MJ/Kg. The better result shown by AlSBA-15 was found to be convincing for the study. Thahir et al. [60] studied pyrolysis of plastic waste under pyrolysis condition. The properties of the fuel were reported which were comparative to the results reported under the pyrolysis condition. Commercial Bentonite clay was used for cracking plastics by Budsaereechai et al. [61]. The calorific value was in the similar range (around 45 MJ/Kg) obtained in this research.

3.8. Mathematical approach

In this section, we obtain the Ti-O2 - [AlSBA-15] interaction as a mathematical model by using van der Waals forces and Lennard-Jones Potential. The Cartesian coordinate (x, y, z) is used as a reference system to model each of the two interacting molecules. The non-bond interaction energy is obtained by summing the interaction energy for each interacting atom,

$$E = \eta_c \eta_l \sum_i \sum_j \phi(\rho) \tag{2}$$

where $\phi(\rho)$ is a potential function for atoms i and j at distanceρ. Here, we apply continuum approximation and atoms are assumed to be uniformly distributed over the surfaces of the two interacting molecules. The double summation in Equation (2) can be replaced by a double integral, which average over the surface of each atom.

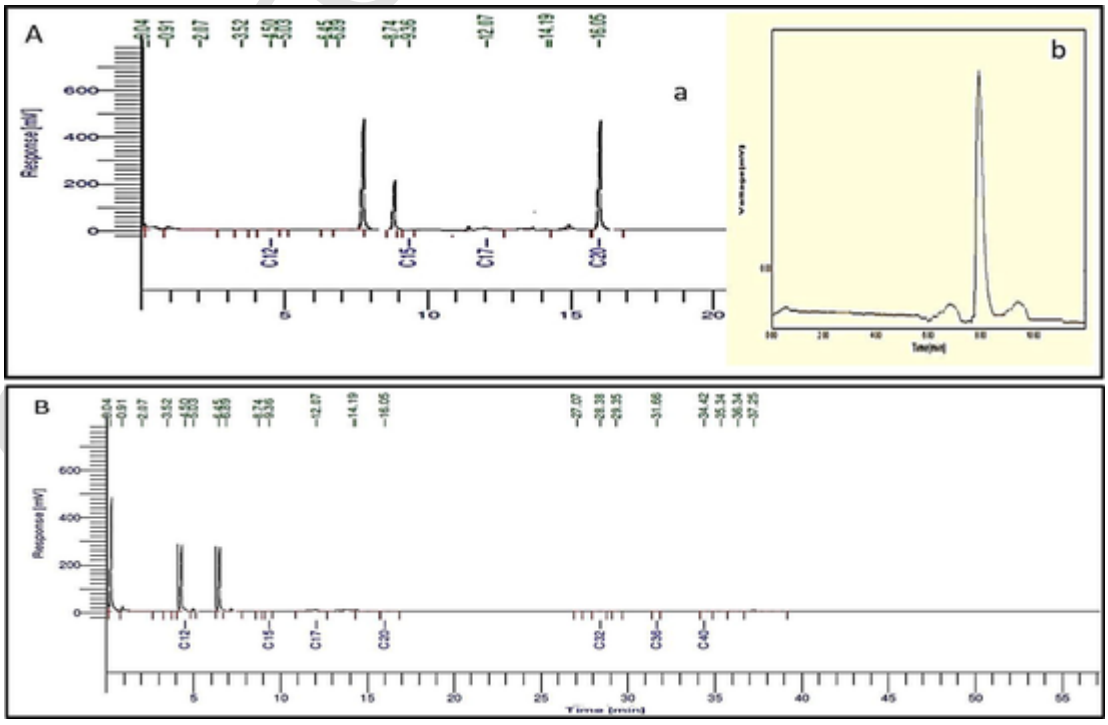

Fig. 9. GC MS spectrum of A) a) Pyrolyzed plastic fuel b) Commercial Diesel B) a) TS-2–PLF.

Table 5
Properties of PLF.

Properties	Standard procedure	Commercial petrol	Pyrolyzed plastic oil	TiO_2 cracked PLF	AlSBA-15 cracked PLF	TS-2 cracked PLF
Flash point (°C)	ASTM D93	20	51.5	61.7	71.5	78.6
Density, 15 °C g/cm^3	ASTM D4052	0.740	0.815	0.800	0.789	0.730
Higher heating value, MJ/Kg	ASTM D240	44.2	40.3	42.7	44.9	47.8
Viscosity @ 40 °C	ASTM D445	0.5 to 0.6	1.98	1.87	1.35	0.98

$$E = \eta_c \eta_l \int\int\int\int \phi(\rho)\, d\delta_c d\delta_l \tag{3}$$

where η_c and η_l are the atomic surface densities for the two molecular structures and ρ is the distance between the two interacting molecules. The classical Lennard-Jones potential for two molecules at a distance ρ apart can be given as:

$$\phi(\rho) = \frac{-A}{\rho^6} + \frac{B}{\rho^{12}} \tag{4}$$

where A and B are the attractive and repulsive constants, respectively. The Lennard-Jones potential and Morse potential used as empirical combining laws, which are given by $\epsilon_{ij} = \sqrt{\epsilon_i \epsilon_j}$ and $\sigma_{ij} = (\sigma_i + \sigma_j)/2$ used to calculate the physical parameters involved in this model; $A = 4\epsilon\sigma^6$ and $B = 4\epsilon\sigma^{12}$, where ϵ is the well depth and σ is the van der Waals diameter [62,63] see Table 6.

TiO_2-[AlSBA-15] has two possible structures as shown in Fig. 10; firstly, it is assumed to be as spherical molecule which located at $(bcos\theta sin\phi, bsin\theta sin\phi, bcos\phi)$, where $\theta \in [-\pi, \pi]$, $\phi \in [0, \pi]$, while the AlSBA-15 is assumed to be cylindrical structure parameterized by $(rcos\theta, rsin\theta, z)$ where $c \in [0, 1]$, $\theta \in [0, 2\pi]$and $z \in [-L/2, L/2]$. the distance ρ_3 between the spherical molecule and a typical point on the cylindrical tube is $\rho^2 = (rcos\theta - bcos\theta sin\phi)^2 + (rsin\theta - bsin\theta sin\phi)^2 + (z - bcos\phi)^2$. From Cox's work *etal*. [64], the interaction energy arising from the interaction between the

Table 6
The Lennard-Jones constants (ϵ: Bond length and σ: Non-Bond distance) and physical parameters involved in this model.

Interaction	ε(Å) [57, 58]	σ(Å) [57, 58]	Attractive ($A = 4\epsilon\sigma^6$)	Repulsive ($B = 4\epsilon\sigma^{12}$)	Configuration Radius (nm)	Atomic Density
Ti-Ti	0.31	3.175	11.89	12,173	0.1761 [62]	0.314 nm^{-1}
O-O	1.11	3.500	34.99	135,169	0.066[61]	0.286 nm^{-1}
Ti-O_2	0.62	3.337	43.08	73,671	≈1 – 1.4 [62]	0.026 nm^{-1}
Al-Al	9.35	4.499	310.14	2,571,956	0.124[61]	0.223 nm^{-1}
Si-Si	7.45	4.295	187.07	1,174,287	0.117[61]	0.233 nm^{-1}
Si-O	2.87	3.889	129.17	654,728	0.118 [61]	0.012 nm^{-3}
Al-Si	8.34	4.397	241.08	1,742,223	0.2331 [61]	0.012 nm^{-3}
Al-SBA-15	5.181	4.194	112.78	613,783	5.908 [63]	0.027 nm^{-2}

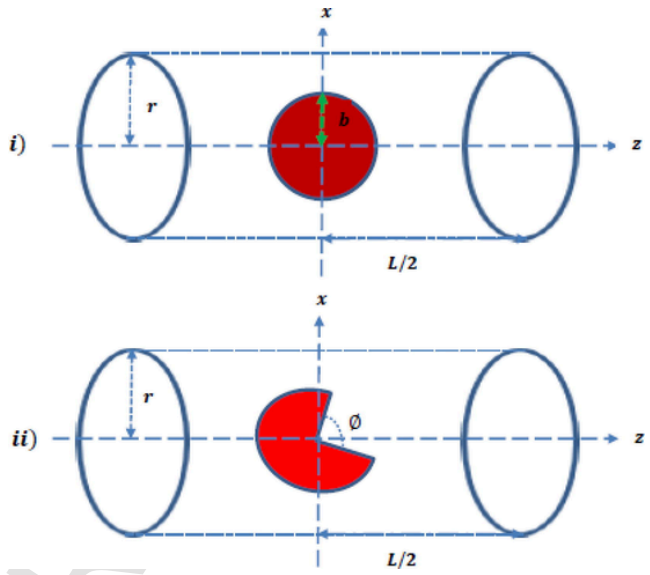

Fig. 10. Schematic geometry for the TiO_2 molecule: i) as spherical shell and ii) as linear molecule (conical) interacting with AlSBA-15 structure as nano-catalyst.

spherical shell of radius b and a typical point on cylindrical tube of radius r as shown in Fig. 10(i) is given by.

$$\begin{aligned} E &= \eta_b \pi b \int\int\int \left[\frac{A}{2}\left(\frac{1}{\rho(\rho+b)^4} - \frac{1}{\rho(\rho-b)^4}\right) - \frac{B}{5}\left(\frac{1}{\rho(\rho+b)^{10}} - \frac{1}{\rho(\rho-b)^{10}}\right)\right] dV \\ &= \eta_b \pi \times b \int_{-L/2}^{L/2}\int_{-\pi}^{\pi}\int_0^1 r^2 \left[\frac{A}{2}\left(\frac{1}{\rho(\rho+b)^4} - \frac{1}{\rho(\rho-b)^4}\right) - \frac{B}{5}\left(\frac{1}{\rho(\rho+b)^{10}} - \frac{1}{\rho(\rho-b)^{10}}\right)\right] dr d\theta dz \end{aligned} \tag{5}$$

where $\eta_b$is the atomic surface density of the spherical shell and $dV = r^2\, dr d\theta dz$ is the element volume. Secondly, we consider one titanium and two oxygen atoms as a linear molecule which is assumed to be located at $(0, 0, tcos\omega + z_0)$, where $t \in [0, 2(\sigma_{OO} + \sigma_{TiO})]$. The distance ρ between the linear chain of carbon atoms and the cylindrical nanotube is given by ${\rho_1}^2 = r^2 + (z - (tcos\omega + z_0))^2$. Thus, by defining D_n as.

$$T_n = r(\sigma_{OO} + \sigma_{TiO}) \int_0^{2(\sigma_{OO}+\sigma_{TiO})} \int_0^{2\pi} \int_{-\infty}^{\infty} \frac{1}{{\rho_1}^{2n}} dz d\omega dt \tag{6}$$

From using the work of AL Garalleh *etal*. [64], the interaction energy can be given, as Fig. 10(ii), by.
$E = \eta_l \eta_c(-AT_3 + BT_6)$, (7).

where $\eta_l$andη_c are the atomic line and the atomic surface densities of the linear chain of atoms (TiO_2 molecule) and the cylindrical group of atoms (AlSBA-15), respectively.

In this section we evaluate the interaction energy of TiO_2 molecule interacting with an AlSBA-15 forming a biofuel nano-catalyst. The well depth ϵ and van der Waals diameter $\sigma$to calculate the attractive and repulsive constants as shown in Table 6. The atomic density foe each interaction molecule calculated as the total number of atoms which are containing the certain structure divided by the surface area or volume of the molecule structure. Thus, the resultant potential energy arising

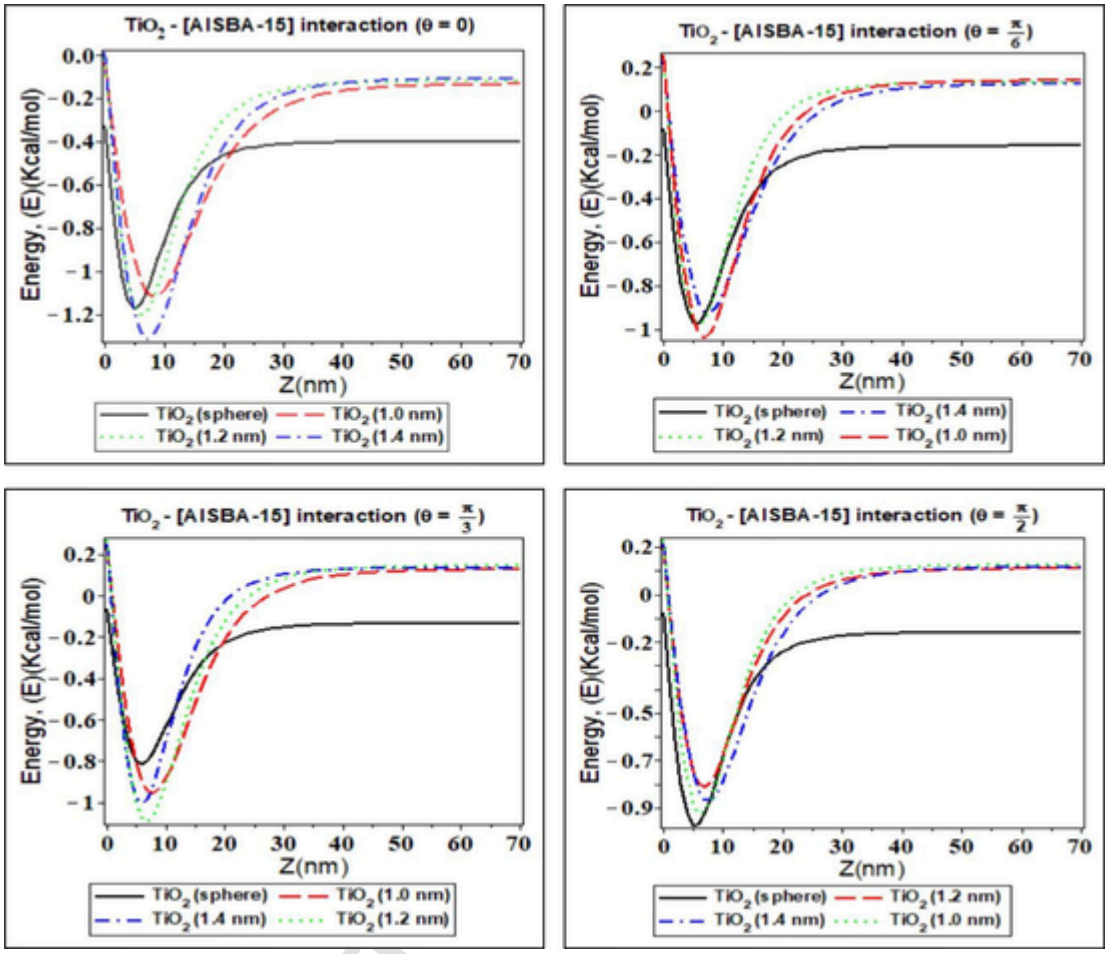

Fig. 11. The magnitude of potential energy arising from TiO_2–[AlSBA-15] interaction.

from the TiO_2-[AlSBA-15] interaction evaluated and plotted based on the angle ∅ that the TiO_2 as linear molecule makes with the z-axis (see Fig. 11). By assuming that $\emptyset = 0, \frac{\pi}{6}, \frac{\pi}{3}$ and $\frac{\pi}{2}$, the numerical results obtained from the TiO2 - [AlSBA-15] interactions (two sub-models) indicate that the obtained minimum energy from the TiO2 as a linear (conical) molecule interacting with AlSBA-15 molecule is −1.34 Kcal/mol when ∅ = 0 (radius of TiO2 is 1.4 *nm*) then followed by π/3, π/6 and π/2 which are −1.09, −1.04 and −0.93 Kcal/mol (-1.04 ≤ E ≤ -1.34 Kcal/mol) being greater than that of the TiO2 considering as spherical molecule of radius b which is in the range of −0.81 ≤ E ≤ -1.17 Kcal/mol.

4. Conclusions

- The thermal vs catalytic pyrolysis condition in cracking LDPEW into PLF was studied.
- TiO_2/AlSBA-15; a nanocomposite was synthesized successfully, and the characterization details confirm the presence of mesoporosity of composite material.
- A desirable range of hydrocarbons (gasoline range) was obtained during catalytic cracking.
- The catalytic activity was in the order of TiO_2 < AlSBA-15 (27) < TiO_2/AlSBA-15 (10%)
- The calorific value of the PLF was in considerable range alike gasoline.
- The TiO_2-[AlSBA-15] interaction is evaluated and plotted by performing the surface and volume integrals for each interacting molecule and based on the orientation angle that TiO_2 molecule makes with the z-axis of AlSBA-15 structure. We have also found out that the minimum energy arising from the TiO_2-[AlSBA-15] as linear – cylindrical interaction which is about −1.34 is greater than that of spherical -cylindrical structure of roughly −1.17 Kcal/mol.
- The numerical results obtained from the TiO2 - [AlSBA-15] interactions (two sub-models) show that the lowest minimum energy is −1.34 Kcal/mol occurs when ∅ = 0 then followed by π/3, π/6 and π/2 which are −1.09, −1.04 and −0.93 Kcal/mol (-1.04 ≤ E ≤ -1.34 Kcal/mol) being greater than that of the TiO_2 considering as a spherical molecule of radius b which is in the range of −0.81 ≤ E ≤ -1.17 Kcal/mol.

Declaration of Competing Interest

The authors declare that they have no known competing financial interests or personal relationships that could have appeared to influence the work reported in this paper.

Acknowledgement

The authors acknowledge that this project was funded by the Deanship of Scientific Research (DSR), University of Business and Technology, Jeddah 21361, Saudi Arabia. The authors would also like to thank Van Lang University, Vietnam for funding this work.

References

[1] Pradeep SA, Iyer RK, Kazan H, Pilla S. Automotive applications of plastics: past, present, and future. Applied Plastics Engineering Handbook Elsevier 2017;651–73.
[2] Reshmy R, Thomas D, Philip E, Paul SA, Madhavan A, Sindhu R, et al. Bioplastic production from renewable lignocellulosic feedstocks: a review. Reviews in

Environmental Science and Bio/Technology 2021;20(1):167–87.
[3] Dou B, Lim S, Kang P, Hwang J, Song S, Yu T-U, et al. Kinetic study in modeling pyrolysis of refuse plastic fuel. Energy Fuels 2007;21(3):1442–7.
[4] Jubinville D, Esmizadeh E, Saikrishnan S, Tzoganakis C, Mekonnen T. A comprehensive review of global production and recycling methods of polyolefin (PO) based products and their post-recycling applications. Sustainable MaterTechnol 2020;25:e00188. https://doi.org/10.1016/j.susmat.2020.e00188.
[5] Sekar M, Ponnusamy VK, Pugazhendhi A, Nižetić S, Praveenkumar TR. Production and utilization of pyrolysis oil from solidplastic wastes: A review on pyrolysis process and influence of reactors design. J Environ Manage 2022;302:114046. https://doi.org/10.1016/j.jenvman.2021.114046.
[6] Zhao P, Xie J, Gu Fu, Sharmin N, Hall P, Fu J. Separation of mixed waste plastics via magnetic levitation. Waste Manage 2018;76:46–54.
[7] Drzyzga O, Prieto A. Plastic waste management, a matter for the 'community'. Microb Biotechnol 2019;12(1):66–8.
[8] Stan F, Stanciu N-V, Fetecau C, Sandu I-L. Mechanical Recycling of Low-Density Polyethylene/Carbon Nanotube Composites and its Effect on Material Properties. J Manuf Sci Eng 2019;141(9):091004.
[9] Vollmer I, Jenks MJF, Roelands MCP, White RJ, Harmelen T, Wild P, et al. Beyond mechanical recycling: Giving new life to plastic waste. Angew Chem Int Ed 2020;59(36):15402–23.
[10] Ramesh P, Vinodh S. State of art review on Life Cycle Assessment of polymers. Int J Sustainable Eng 2020;13(6):411–22.
[11] Gowthaman N, Lim H, Sreeraj T, Amalraj A, Gopi S. Advantages of biopolymers over synthetic polymers: social, economic, and environmental aspects. Biopolymers and their Industrial Applications Elsevier 2021;351–72.
[12] Das P, Tiwari P. The effect of slow pyrolysis on the conversion of packaging waste plastics (PE and PP) into fuel. Waste Manage 2018;79:615–24.
[13] Olivera M, Musso M, De León A, Volonterio E, Amaya A, Tancredi N, et al. Catalytic assessment of solid materials for the pyrolytic conversion of low-density polyethylene into fuels. Heliyon 2020;6(9):e05080. https://doi.org/10.1016/j.heliyon.2020.e05080.
[14] Nanda S, Berruti F. Thermochemical conversion of plastic waste to fuels: a review. Environ Chem Lett 2021;19(1):123–48.
[15] Mangesh VL, Padmanabhan S, Tamizhdurai P, Ramesh A. Experimental investigation to identify the type of waste plastic pyrolysis oil suitable for conversion to diesel engine fuel. J Cleaner Prod 2020;246:119066. https://doi.org/10.1016/j.jclepro.2019.119066.
[16] Mahmudul HM, Hagos FY, Mamat R, Adam AA, Ishak WFW, Alenezi R. Production, characterization and performance of biodiesel as an alternative fuel in diesel engines–A review. Renew Sustain Energy Rev 2017;72:497–509.
[17] Quesada L, Pérez A, Godoy V, Peula FJ, Calero M, Blázquez G. Optimization of the pyrolysis process of a plastic waste to obtain a liquid fuel using different mathematical models. Energy Convers Manage 2019;188:19–26.
[18] Utami M, Wijaya K, Trisunaryanti W. Pt-promoted sulfated zirconia as catalyst for hydrocracking of LDPE plastic waste into liquid fuels. Mater Chem Phys 2018;213:548–55.
[19] Sharuddin S, Abnisa F, Daud W, Aroua M. Pyrolysis of plastic waste for liquid fuel production as prospective energy resource. *IOP Conference Series: Materials Science and Engineering*. 334. IOP Publishing; 2018:012001.
[20] Sekar M, Praveenkumar TR, Dhinakaran V, Gunasekar P, Pugazhendhi A. Combustion and emission characteristics of diesel engine fueled with nanocatalyst and pyrolysis oil produced from the solid plastic waste using screw reactor. J Cleaner Prod 2021;318:128551. https://doi.org/10.1016/j.jclepro.2021.128551.
[21] Zhang Y, Duan D, Lei H, Villota E, Ruan R. Jet fuel production from waste plastics via catalytic pyrolysis with activated carbons. Appl Energy 2019;251:113337. https://doi.org/10.1016/j.apenergy.2019.113337.
[22] Sophonrat N, Sandström L, Zaini IN, Yang W. Stepwise pyrolysis of mixed plastics and paper for separation of oxygenated and hydrocarbon condensates. Appl Energy 2018;229:314–25.
[23] Gear M, Sadhukhan J, Thorpe R, Clift R, Seville J, Keast M. A life cycle assessment data analysis toolkit for the design of novel processes–A case study for a thermal cracking process for mixed plastic waste. J Cleaner Prod 2018;180:735–47.
[24] Anuar Sharuddin SD, Abnisa F, Wan Daud WMA, Aroua MK. A review on pyrolysis of plastic wastes. Energy Convers Manage 2016;115:308–26.
[25] Basu P. Biomass gasification, pyrolysis and torrefaction: practical design and theory. Academic press; 2018.
[26] Carmo-Calado L, Hermoso-Orzáez MJ, Mota-Panizio R, Guilherme-Garcia B, Brito P. Co-combustion of waste tires and plastic-rubber wastes with biomass technical and environmental analysis. Sustainability 2020;12(3):1036.
[27] Kasar P, Sharma DK, Ahmaruzzaman M. Thermal and catalytic decomposition of waste plastics and its co-processing with petroleum residue through pyrolysis process. J Cleaner Prod 2020;265:121639. https://doi.org/10.1016/j.jclepro.2020.121639.
[28] Nwankwor PE, Onuigbo IO, Chukwuneke CE, Yahaya MF, Agboola BO, Jahng WJ. Synthesis of gasoline range fuels by the catalytic cracking of waste plastics using titanium dioxide and zeolite. International Journal of Energy and Environmental Engineering 2021;12(1):77–86.
[29] Xu X, Ren H, Li H, Liu J, Cao P, Wang X. Microstructure evolution and plastic mechanism in deformation of bulk amorphous Al2O3-ZrO2-Y2O3. Ceram Int 2019;45(12):14789–93.
[30] Yu F, Gao L, Wang W, Zhang G, Ji J. Bio-fuel production from the catalytic pyrolysis of soybean oil over Me-Al-MCM-41 (Me= La, Ni or Fe) mesoporous materials. J Anal Appl Pyrol 2013;104:325–9.
[31] García RA, Serrano DP, Otero D. Catalytic cracking of HDPE over hybrid zeolitic–mesoporous materials. J Anal Appl Pyrol 2005;74(1–2):379–86.
[32] Chi Y, Xue J, Zhuo J, Zhang D, Liu Mi, Yao Q. Catalytic co-pyrolysis of cellulose and polypropylene over all-silica mesoporous catalyst MCM-41 and Al-MCM-41. Sci Total Environ 2018;633:1105–13.
[33] Socci J, Osatiashtiani A, Kyriakou G, Bridgwater T. The catalytic cracking of sterically challenging plastic feedstocks over high acid density Al-SBA-15 catalysts. Appl Catal A 2019;570:218–27.
[34] Zhao Y, Wang W, Jing X, Gong X, Wen H, Deng Y. Catalytic cracking of polypropylene by using Fe-SBA-15 synthesized in an acid-free medium for production of light hydrocarbon oils. J Anal Appl Pyrol 2020;146:104755. https://doi.org/10.1016/j.jaap.2019.104755.
[35] Munir D, Usman MR. Catalytic hydropyrolysis of a model municipal waste plastic mixture over composite USY/SBA-16 catalysts. J Anal Appl Pyrol 2018;135:44–53.
[36] Ge S, Ganesan R, Sekar M, Xia C, Shanmugam S, Alsehli M, et al. Blending and emission characteristics of biogasoline produced using CaO/SBA-15 catalyst by cracking used cooking oil. Fuel 2022;307:121861. https://doi.org/10.1016/j.fuel.2021.121861.
[37] Shi Z, Wu C, Wu Y, Liu H, Xu G, Deng J, et al. Optimization of epoxypinane synthesis by silicotungstic acid supported on SBA-15 catalyst using response surface methodology. Sci Adv Mater 2019;11(5):699–707.
[38] Wan MM, Qian WJ, Lin WG, Zhou Y, Zhu JH. Multiple functionalization of SBA-15 mesoporous silica in one-pot: fabricating an aluminum-containing plugged composite for sustained heparin release. J Mater Chem B 2013;1(32):3897–905.
[39] Kolli MK, Palani E, Govindasamy C, Katta VR. Highly efficient one-pot synthesis of α-aminophosphonates using nanoporous AlSBA-15 catalyst in a three-component system. Res Chem Intermed 2020;46(2):1047–64.
[40] Guo Q-Y, Yan X-Y, Zhang W, Li X-H, Xu Y, Dai S, et al. Ordered Mesoporous Silica Pyrolyzed from Single-Source Self-Assembled Organic-Inorganic Giant Surfactants. J Am Chem Soc 2021;143(33):12935–42.
[41] Marques J, Gomes TD, Forte MA, Silva RF, Tavares CJ. A new route for the synthesis of highly-active N-doped TiO2 nanoparticles for visible light photocatalysis using urea as nitrogen precursor. Catal Today 2019;326:36–45.
[42] Jaroszewska K, Fedyna M, Trawczyński J. Hydroisomerization of long-chain n-alkanes over Pt/AlSBA-15+ zeolite bimodal catalysts. Appl Catal B 2019;255:117756. https://doi.org/10.1016/j.apcatb.2019.117756.
[43] SHINDO T, KOIZUMI N, HATAKEYAMA K, IKEUCHI T. Post-synthesis of TiO2 Dispersed inside the Pore Channels of SBA-15 and its Photocatalytic Activity for the Degradation of Methylene Blue. International Journal of the Society of Materials Engineering for Resources 2011;18(1):11–7.
[44] Chen S-Y, Mochizuki T, Abe Y, Toba M, Yoshimura Y. Production of high-quality biodiesel fuels from various vegetable oils over Ti-incorporated SBA-15 mesoporous silica. Catal Commun 2013;41:136–9.
[45] Das P, Tiwari P. Thermal degradation study of waste polyethylene terephthalate (PET) under inert and oxidative environments. Thermochim Acta 2019;679:178340. https://doi.org/10.1016/j.tca.2019.178340.
[46] Zheng Y, Tao L, Yang X, Huang Y, Liu C, Zheng Z. Study of the thermal behavior, kinetics, and product characterization of biomass and low-density polyethylene co-pyrolysis by thermogravimetric analysis and pyrolysis-GC/MS. J Anal Appl Pyrol 2018;133:185–97.
[47] Ochoa A, Bilbao J, Gayubo AG, Castaño P. Coke formation and deactivation during catalytic reforming of biomass and waste pyrolysis products: a review. Renew Sustain Energy Rev 2020;119:109600. https://doi.org/10.1016/j.rser.2019.109600.
[48] Yu L, Farinmade A, Ajumobi O, Su Y, John VT, Valla JA. MCM-41/ZSM-5 composite particles for the catalytic fast pyrolysis of biomass. Appl Catal A 2020;602:117727. https://doi.org/10.1016/j.apcata.2020.117727.
[49] Wang Y, Ke L, Peng Y, Yang Qi, Du Z, Dai L, et al. Characteristics of the catalytic fast pyrolysis of vegetable oil soapstock for hydrocarbon-rich fuel. Energy Convers Manage 2020;213:112860. https://doi.org/10.1016/j.enconman.2020.112860.
[50] Vu XH, Armbruster U. Catalytic cracking of triglycerides over micro/mesoporous zeolitic composites prepared from ZSM-5 precursors with varying aluminum contents. Reaction kinetics, mechanisms and catalysis 2018;125(1):381–94.
[51] Shirasaki Y, Nasu H, Hashimoto T, Ishihara A. Effects of types of zeolite and oxide and preparation methods on dehydrocyclization-cracking of soybean oil using hierarchical zeolite-oxide composite-supported Pt/NiMo sulfided catalysts. Fuel Process Technol 2019;194:106109. https://doi.org/10.1016/j.fuproc.2019.05.032.
[52] Ganesan R, Thiripuranthagan S, Subba S. Synthesis and characterization of core-shell modeled AlMCM-48/HZSM-5 composite catalyst and studies on its catalytic activity in cracking of pongamia oil into bio liquid products. Bioenergy Res 2019;12(2):388–99.
[53] Hossain M, Siddik Bhuyan Md, Md Ashraful Alam A, Seo Y. Optimization of biodiesel production from waste cooking oil using S-TiO2/SBA-15 heterogeneous acid catalyst. Catalysts 2019;9(1):67.;9(1):67. https://doi.org/10.3390/catal9010067.
[54] Klimova T, Gutiérrez O, Lizama L, Amezcua J. Advantages of ZrO_2-and TiO_2–SBA-15 mesostructured supports for hydrodesulfurization catalysts over pure TiO_2, ZrO_2 and SBA-15. Microporous Mesoporous Mater 2010;133(1–3):91–9.
[55] Hartati, Trisunaryanti W, Mukti RR, Kartika IA, Firda PBD, Sumbogo SD, et al. Highly selective hierarchical ZSM-5 from kaolin for catalytic cracking of Calophyllum inophyllum oil to biofuel. J Energy Inst 2020;93(6):2238–46.
[56] Hu W, Wang H, Lin H, Zheng Y, Ng S, Shi M, et al. Catalytic decomposition of oleic acid to fuels and chemicals: Roles of catalyst acidity and basicity on product distribution and reaction pathways. Catalysts 2019;9(12):1063. https://doi.org/10.3390/catal9121063.
[57] Cao X, Li Lu, Shitao Yu, Liu S, Hailong Yu, Qiong Wu, et al. Catalytic conversion of waste cooking oils for the production of liquid hydrocarbon biofuels using in-situ

coating metal oxide on SBA-15 as heterogeneous catalyst. J Anal Appl Pyrol 2019; 138:137–44.
[58] Yousef S, Eimontas J, Striūgas N, Zakarauskas K, Praspaliauskas M, Abdelnaby MA. Pyrolysis kinetic behavior and TG-FTIR-GC–MS analysis of metallised food packaging plastics. Fuel 2020;282:118737. https://doi.org/10.1016/j.fuel.2020.118737.
[59] Dwivedi U, Naik SN, Pant KK. High quality liquid fuel production from waste plastics via two-step cracking route in a bottom-up approach using bi-functional Fe/HZSM-5 catalyst. Waste Manage 2021;132:151–61.
[60] Thahir R, Altway A, Juliastuti SR, Susianto. Production of liquid fuel from plastic waste using integrated pyrolysis method with refinery distillation bubble cap plate column. Energy Rep 2019;5:70–7.
[61] Budsaereechai S, Hunt AJ, Ngernyen Y. Catalytic pyrolysis of plastic waste for the production of liquid fuels for engines. RSC Adv 2019;9(10):5844–57.
[62] Rappe AK, Casewit CJ, Colwell KS, Goddard WA, Skiff WM. UFF, a full periodic table force field for molecular mechanics and molecular dynamics simulations. J Am Chem Soc 1992;114(25):10024–35.
[63] Cottrell LT. The strengths of chemical bonds. Academic Press; 1958.
[64] Cox BJ, Thamwattana N, Hill JM. Mechanics of atoms and fullerenes in single-walled carbon nanotubes. Proceedings of the Royal Society A: Mathematical, Physical and Engineering Sciences 2006;463(2078):461–77.